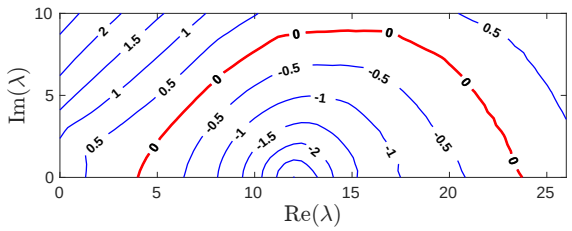

FIG. 6. Stability function $\psi(\lambda)$ for the *AISync* system in Fig. 3.

of $\psi(\lambda)$, which has a bounded stability region $\{\lambda \in \mathbb{C} \,|\, \psi(\lambda) < 0\}$.

For a given combination of a and b, we obtain $\Psi_=$ and $\Psi_\neq$, which are shown in Fig. 3(b). Note that for this example there are only two distinct homogeneous systems and two distinct heterogeneous systems. One of these heterogeneous systems is shown in Fig. 3(a). We also note that $\Psi_= > 0$ and $\Psi_\neq < 0$ are equivalent to the conditions (C1)′ and (C2)′ in Appendix D, respectively. For each combination of a and b satisfying both conditions [on a grid covering Fig. 3(b) with a resolution of 0.2], we additionally run 24 direct simulations of Eq. (2) for 200 time units. The initial condition $\boldsymbol{x}_\ell^{(i)}(0)$ for each subnode is chosen randomly and independently from the uniform distribution in the region $[0, 10] \times [0, 10] \times [0, 10]$ of its state space. The results confirm that the synchronization error e defined in Eq. (D1) and averaged over the last 100 time units does not fall below 10^{-3} in all 24 runs for both homogeneous systems, providing solid evidence that the system satisfies the *AISync* condition (C1) for these combinations of a and b. Since $\Psi_\neq < 0$ implies (C2)′ and thus (C2), this confirms *AISync* in the region shaded purple in Fig. 3(b).

The initial condition for the sample trajectory in Fig. 3(c) is chosen randomly within a distance of 10^{-3} from the synchronous state. The trajectory is then computed by integrating the system with all nodes green for $t \leq 25$, instantaneously switching the direction of the sublink between subnodes $2'$ and $2''$, and then continuing to integrate for $25 \leq t \leq 50$.

Appendix F: Sampling protocol used in Fig. 4

We randomly sample systems whose network structure $A^{(\alpha)}$ is a circulant graph (with directed links of possibly multiple types) of given size N and external sublink in-degree D (i.e., the total number of sublinks received by the subnodes of a given node). Each of the D sublinks coming into node 1 is chosen randomly; it connects a random subnode chosen uniformly from the other $N-1$ nodes to a random subnode chosen uniformly from node 1. The incoming sublinks into nodes 2 to N are then chosen to precisely match those coming into node 1, which ensures that the network structure is a circulant graph. This simultaneously specifies $A^{(\alpha)}$ and $B^{(\alpha)}$ defining the system. To determine $\sigma_\neq$, $\sigma_=$, and r for this system, we calculate the eigenspread σ of the monolayer network representation for all the possible internal sublink configurations $F^{(i)}$, chosen here from the binary set $\{\left(\begin{smallmatrix}0&1\\0&0\end{smallmatrix}\right), \left(\begin{smallmatrix}0&0\\1&0\end{smallmatrix}\right)\}$. For each combination of N and D, we generate a sample of 4,000 such systems to compute the fraction of *AISync*-favoring networks.

Appendix G: Approximate symmetry in Fig. 4(a)

The approximate symmetry with respect to the vertical line at density 0.5 observed in Fig. 4(a) can be explained using the notion of network complement. The complement of a given (unweighted) network with adjacency matrix $\widetilde{A} = (\widetilde{A}_{jj'})$ is defined as the network having the adjacency matrix $\widetilde{A}^c = (\widetilde{A}^c_{jj'})$ given by

$$\widetilde{A}^c_{jj'} := (1 - \widetilde{A}_{jj'})(1 - \delta_{jj'}). \tag{G1}$$

The external sublink density of a network and its complement add up to one, placing them symmetrically about the vertical line at density 0.5 in Fig. 4(a). When the nontrivial Laplacian eigenvalues of the network and its complement, which we denote $\lambda_2, \ldots, \lambda_n$ and $\lambda^c_2, \ldots, \lambda^c_n$, respectively, are both indexed in the order of increasing real part, they are related by $\lambda_j + \lambda^c_{n+2-j} = n$ [8]. This implies that, if σ is the eigenvalue spread for a monolayer network with given internal sublink configurations $F^{(i)}$, then the spread for its complement is given by

$$\sigma^c = \frac{\widetilde{m}\sigma}{n(n-1) - \widetilde{m}}, \tag{G2}$$

where $\widetilde{m} := \sum_j \sum_{j' \neq j} \widetilde{A}_{jj'}$ is the number of directed links in the network $\widetilde{A}$. Now consider two systems with n subnodes and adjacency matrices $\widetilde{A}_1$ and $\widetilde{A}_2$, whose σ values are σ_1 and σ_2, respectively. If we denote the σ values of the complement of these systems by σ^c_1 and σ^c_2, respectively, we have

$$\frac{\sigma_1}{\sigma_2} = \frac{\sigma^c_1}{\sigma^c_2} \tag{G3}$$

when $\widetilde{A}_1$ and $\widetilde{A}_2$ have the same number of directed links, i.e., $\widetilde{m}_1 = \widetilde{m}_2$. It follows from Eq. (G2) that if $\widetilde{A}_1$ is the best homogeneous system and $\widetilde{A}_2$ the best heterogeneous system for a given external connection pattern with density x, then their complements are the best homogeneous and heterogeneous system for an external connection pattern with density $1 - x$. Thus, the value of *AISync* strength r is the same at density x and $1 - x$. The symmetry, however, is not perfect between sparse and dense parts of the plot, since we exclude the cases in which the network is not synchronizable (i.e., we require $\min_{j \geq 2} \mathrm{Re}(\lambda_j) > 0$), the effect of which is not symmetric between sparse and dense cases.

[1] Juan G Restrepo, Edward Ott, and Brian R Hunt, "Spatial patterns of desynchronization bursts in networks," Phys. Rev. E **69**, 066215 (2004).

[2] Jie Sun, Erik M Bollt, and Takashi Nishikawa, "Master stability functions for coupled nearly identical dynamical systems," Europhys. Lett. **85**, 60011 (2009).

[3] Takashi Nishikawa, Adilson E Motter, Ying-Cheng Lai, and Frank C Hoppensteadt, "Heterogeneity in oscillator networks: Are smaller worlds easier to synchronize?" Phys. Rev. Lett. **91**, 014101 (2003).

[4] Michael Denker, Marc Timme, Markus Diesmann, Fred Wolf, and Theo Geisel, "Breaking synchrony by heterogeneity in complex networks," Phys. Rev. Lett. **92**, 074103 (2004).

[5] Luca Donetti, Pablo I Hurtado, and Miguel A Munoz, "Entangled networks, synchronization, and optimal network topology," Phys. Rev. Lett. **95**, 188701 (2005).

[6] Adilson E Motter, Changsong Zhou, and Jürgen Kurths, "Network synchronization, diffusion, and the paradox of heterogeneity," Phys. Rev. E **71**, 016116 (2005).

[7] Changsong Zhou and Jürgen Kurths, "Dynamical weights and enhanced synchronization in adaptive complex networks," Phys. Rev. Lett. **96**, 164102 (2006).

[8] Takashi Nishikawa and Adilson E Motter, "Network synchronization landscape reveals compensatory structures, quantization, and the positive effect of negative interactions," Proc. Natl. Acad. Sci. U.S.A. **107**, 10342–10347 (2010).

[9] Takashi Nishikawa and Adilson E. Motter, "Symmetric states requiring system asymmetry," Phys. Rev. Lett. **117**, 114101 (2016).

[10] Yoshiki Kuramoto and Dorjsuren Battogtokh, "Coexistence of coherence and incoherence in nonlocally coupled phase oscillators," Nonlinear Phenom. Complex Syst. **5**, 380 (2002).

[11] Daniel M Abrams and Steven H Strogatz, "Chimera states for coupled oscillators," Phys. Rev. Lett. **93**, 174102 (2004).

[12] Norman Biggs, *Algebraic graph theory* (Cambridge university press, 1993).

[13] Mark J Panaggio and Daniel M Abrams, "Chimera states: coexistence of coherence and incoherence in networks of coupled oscillators," Nonlinearity **28**, R67 (2015).

[14] The On-Line Encyclopedia of Integer Sequences, published electronically at https://oeis.org, 2007, Sequence A006799.

[15] Thomas Dahms, Judith Lehnert, and Eckehard Schöll, "Cluster and group synchronization in delay-coupled networks," Phys. Rev. E **86**, 016202 (2012).

[16] Louis M Pecora, Francesco Sorrentino, Aaron M Hagerstrom, Thomas E Murphy, and Rajarshi Roy, "Cluster synchronization and isolated desynchronization in complex networks with symmetries," Nat. Commun. **5** (2014).

[17] Charo I. del Genio, Jesús Gómez-Gardeñes, Ivan Bonamassa, and Stefano Boccaletti, "Synchronization in networks with multiple interaction layers," Sci. Adv. **2** (2016).

[18] Jianxi Gao, Sergey V Buldyrev, H Eugene Stanley, and Shlomo Havlin, "Networks formed from interdependent networks," Nature Phys. **8**, 40–48 (2012).

[19] Sergio Gomez, Albert Diaz-Guilera, Jesus Gomez-Gardeñes, Conrad J Perez-Vicente, Yamir Moreno, and Alex Arenas, "Diffusion dynamics on multiplex networks," Phys. Rev. Lett. **110**, 028701 (2013).

[20] Manlio De Domenico, Albert Solé-Ribalta, Emanuele Cozzo, Mikko Kivelä, Yamir Moreno, Mason A Porter, Sergio Gómez, and Alex Arenas, "Mathematical formulation of multilayer networks," Phys. Rev. X **3**, 041022 (2013).

[21] Stefano Boccaletti, Ginestra Bianconi, Regino Criado, Charo I Del Genio, Jesús Gómez-Gardeñes, Miguel Romance, Irene Sendiña-Nadal, Zhen Wang, and Massimiliano Zanin, "The structure and dynamics of multilayer networks," Phys. Rep. **544**, 1–122 (2014).

[22] Manlio De Domenico, Clara Granell, Mason A Porter, and Alex Arenas, "The physics of spreading processes in multilayer networks," Nature Phys. **12**, 901–906 (2016).

[23] Xiyun Zhang, Stefano Boccaletti, Shuguang Guan, and Zonghua Liu, "Explosive synchronization in adaptive and multilayer networks," Phys. Rev. Lett. **114**, 038701 (2015).

[24] Lucia Valentina Gambuzza, Mattia Frasca, and Jesus Gomez-Gardeñes, "Intra-layer synchronization in multiplex networks," Europhys. Lett. **110**, 20010 (2015).

[25] Louis M Pecora and Thomas L Carroll, "Master stability functions for synchronized coupled systems," Phys. Rev. Lett. **80**, 2109 (1998).

[26] Zhongkui Li, Zhisheng Duan, Guanrong Chen, and Lin Huang, "Consensus of multiagent systems and synchronization of complex networks: a unified viewpoint," IEEE Trans. Circuits Syst. I, Reg. Papers **57**, 213–224 (2010).

[27] Aaron M Hagerstrom, Thomas E Murphy, Rajarshi Roy, Philipp Hövel, Iryna Omelchenko, and Eckehard Schöll, "Experimental observation of chimeras in coupled-map lattices," Nature Phys. **8**, 658–661 (2012).

[28] Takashi Nishikawa and Adilson E Motter, "Synchronization is optimal in nondiagonalizable networks," Phys. Rev. E **73**, 065106 (2006).

[29] Martin Golubitsky and Ian Stewart, "Rigid patterns of synchrony for equilibria and periodic cycles in network dynamics," Chaos **26**, 094803 (2016).

[30] Vincenzo Nicosia, Miguel Valencia, Mario Chavez, Albert Díaz-Guilera, and Vito Latora, "Remote synchronization reveals network symmetries and functional modules," Phys. Rev. Lett. **110**, 174102 (2013).

[31] Alan Wolf, Jack B Swift, Harry L Swinney, and John A Vastano, "Determining lyapunov exponents from a time series," Physica D **16**, 285–317 (1985).

Supplemental Material

Asymmetry-Induced Synchronization in Oscillator Networks

Yuanzhao Zhang, Takashi Nishikawa, and Adilson E. Motter

Appendix S1: Example of *AISync* with unbounded stability region

Figure S1 shows another example of *AISync* using systems in which subnode dynamics is the same Lorenz oscillator as in Fig. 2, but with a different coupling function [leading to a different stability function $\psi(\lambda)$] and a different symmetric network. We use a three-node symmetric network with a single link type [with the corresponding coupling matrix $B^{(1)} = \left(\begin{smallmatrix} 0 & b \\ 0 & 0 \end{smallmatrix}\right)$], as can be seen in Fig. S1(a), where the monolayer representation of an example heterogenous system is shown. The coupling matrix $F^{(i)}$ for internal sublinks are chosen from the quaternary set $\{\left(\begin{smallmatrix} 0 & 0 \\ 0 & 0 \end{smallmatrix}\right), \left(\begin{smallmatrix} 0 & a \\ 0 & 0 \end{smallmatrix}\right), \left(\begin{smallmatrix} 0 & 0 \\ a & 0 \end{smallmatrix}\right), \left(\begin{smallmatrix} 0 & a \\ a & 0 \end{smallmatrix}\right)\}$, so there are four distinct homogeneous systems. Two of them have $\lambda_2 = 0$ (and thus are not synchronizable), and one of the remaining ones is always more stable (i.e., smaller Ψ) than the other in the range of a and b considered in Fig. S1.

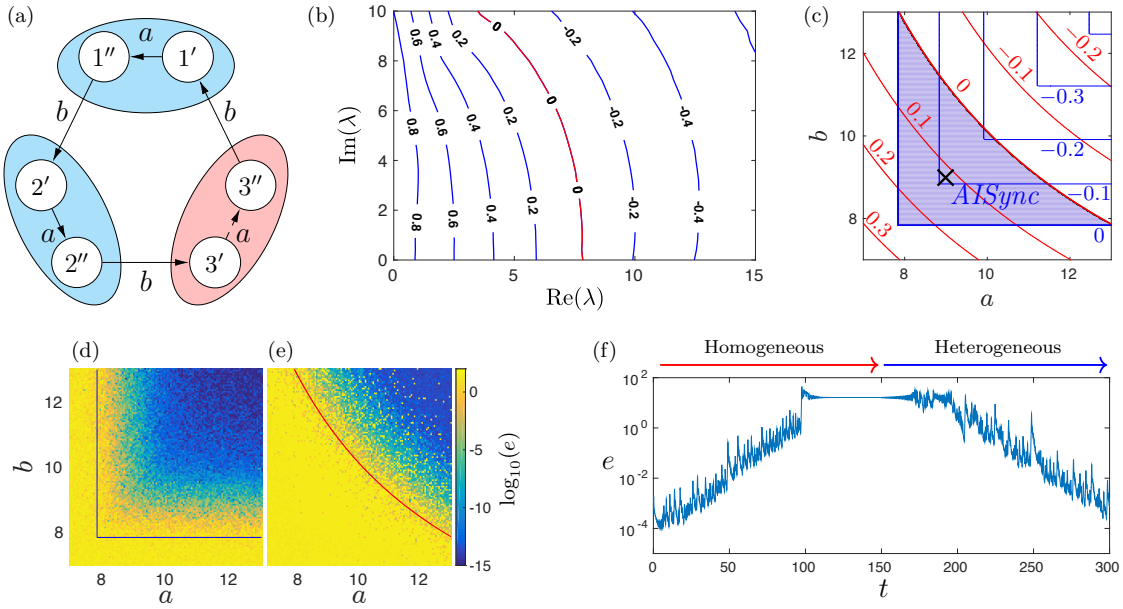

FIG. S1. Example of *AISync* systems that has unbounded stability region. The subnodes are identical Lorenz oscillators, coupled to each other through the first component of their state vectors. (a) Symmetric network of $N = 3$ nodes, with $L = 2$ subnodes per node, shown in the monolayer network representation for a specific heterogeneous system (when the dashed sublink does not exist). If we add the dashed sublink, the system becomes homogeneous. (b) Contour curves for the stability function $\psi(\lambda)$ in the complex plane. The stability region consists of all points to the right of the red curve (corresponding to $\psi = 0$) and thus is unbounded. (c) Contour curves for the MTLE for the homogeneous (red) and heterogeneous (blue) systems as a function of parameters a and b. The region of *AISync* is shaded light purple. (d, e) Synchronization error e after 200 time units for the heterogeneous (d) and the homogeneous (e) system. (f) Time evolution of the synchronization error e for the system at $a = b = 9$ [the cross symbol in (c)] undergoing a switch from being homogeneous to being heterogeneous at $t = 150$ [through the removal of the internal sublink in node 3].

The more stable homogeneous system is the one with the dashed sublink in Fig. S1(a). Among the heterogeneous systems, the one with the smallest value of σ is the one without the dashed sublink in Fig. S1(a), which is optimal (i.e., $\sigma = 0$). We thus have just one homogeneous system and one heterogeneous system to compare. For the coupling function, we use $\boldsymbol{h}(\boldsymbol{x}) = (x_1, 0, 0)^T$, which leads to the stability function $\psi(\lambda)$ shown in Fig. S1(b). Unlike the example in Fig. 2, the stable region for this example (the region to the right of the red curve) is unbounded. Using this $\psi(\lambda)$, we calculate the MTLEs for the homogeneous and heterogeneous systems, which are shown in Fig. S1(c) as functions of parameters a and b. We confirm that the global stability also follows the same trend by integrating Eq. (2) directly for 200 time units from a random initial condition and then computing the synchronization error e defined in Eq. (D1). The result is shown in Fig. S1(d), where we see that e behaves similarly as the MTLE. Figure S1(e) shows the synchronization error e for a typical trajectory of the system with $a = b = 9$ [marked by black cross in Fig. S1(c)],